

# A Large Eddy Simulation framework to assess wind farm power maximization strategies: Validation of maximization by yawing

M Draper <sup>1</sup>, A Guggeri <sup>1</sup>, B López <sup>1</sup>, A Díaz <sup>1</sup>, F Campagnolo <sup>2</sup>, G Usera <sup>1</sup>

<sup>1</sup> Facultad de Ingeniera, Universidad de la Repblica, Julio Herrera y Resissig 565, Montevideo, Uruguay

<sup>2</sup> Wind Energy Institute, Technische Universität München, Boltzmannstraße 15, D-85748 Garching bei München, Germany

E-mail: mdraper@fing.edu.uy

**Abstract.** Recently, there has been an increasing interest in the academic community as well as in the industrial sector about the operation and control of a wind farm at a farm level. This new paradigm has different purposes, from maximizing power production through wake modulation to active power control. The former has been extensively analyzed with numerical or physical modelling, finding in general an improvement in the power production by yawing the wind turbine rotors. The aim of the present paper is to compare both approaches, by taking into account results from state of the art numerical simulations and wind tunnel campaigns. A case with three model wind turbines subject to an atmospheric boundary layer like inflow condition will be studied.

## 1. Introduction

Wind energy has become a mature technology, with a growth rate close to 12% between 2015 and 2016, achieving almost 466 GW of installed capacity [1]. Nevertheless there are still open challenges to further continue its development [2]. Among them, wind farm control to maximize the power production of a whole wind farm has received special attention in the past few years. Several studies have been performed in order to increase the power production of a group of wind turbines, taking into account different approaches, from simplified and reduced order physical models to statistical and more complex models (see for instance [3, 4, 5, 6, 7]). In order to validate the proposed algorithms two alternatives have been used: physical experimental campaigns in wind tunnels and numerical simulations with high fidelity models. Regarding the former, in [6] the physical setup analyzed in this paper is used to evaluate a closed loop control to maximize the total power production of three model wind turbines subject to an atmospheric boundary layer (ABL) like inflow condition, to accomplish this goal a gradient-based extremum seeking control algorithm is developed. In a similar fashion, a wind tunnel setup consisting of six model wind turbines subject to a non-turbulent uniform inflow condition is considered in [7] to assess the capability of an algorithm based on a Gaussian Process Regression to maximize the total energy capture. Regarding high-fidelity validations, in [4] a two-turbine case is studied with a high-fidelity model [8] to assess different strategies to mitigate the wake in order to



maximize the power production. Several configurations are evaluated, varying yaw, position or tilt of the upstream wind turbine, finding a good potential for power improvement. Several studies have been presented using a high-fidelity numerical framework to validate an algorithm aim to maximize energy capture, see for instance [3, 9, 10]. In [11] axial-induction-based and wake redirection-based strategies are compared, finding for the analyzed case that the wake redirection-based strategy has a larger potential improvement.

From the above, it is interesting to evaluate a high-fidelity numerical framework under several yaw settings, comparing the results with wind tunnel measurements. The aim of the present paper is to assess the capability of a validated numerical framework, under different inflow conditions and wind turbine setups [12, 13, 14, 15], to simulate accurately the flow over a group of wind turbines operating under non-optimal conditions focused on maximizing the overall power production. To accomplish this, a state-of-the-art wind tunnel campaign is chosen as validation case, that consists of three model wind turbines separated  $4D$  in the streamwise direction and with a lateral shift of half a diameter. The paper is centered on the power computation of each yaw setting, particularly in finding the optimum yaw setting comparing experimental and numerical results. In addition to this, a comparison of the wind fields between two selected configurations is performed.

The paper is organized as follows: Section 2 describes the experimental setup, Section 3 presents a brief description of the numerical solver and the numerical setup while Section 4 presents the main results, first presenting a deeper comparison between numerical and experimental data for two yaw settings and then a comparison of the energy capture of several configurations, and conclusions are given in Section 5.

## 2. Experimental setup

The experimental setup is shown in Figure 1. It consists of three wind turbine models, in the following named G1s, whose rotor diameter  $D$  is 1.1 m and which were arranged with a longitudinal and lateral spacing of  $4D$  and  $0.5D$ , respectively. The same figure also depicts the two short-range WindScanners which were employed to get a reliable high resolution mapping of the wind field.

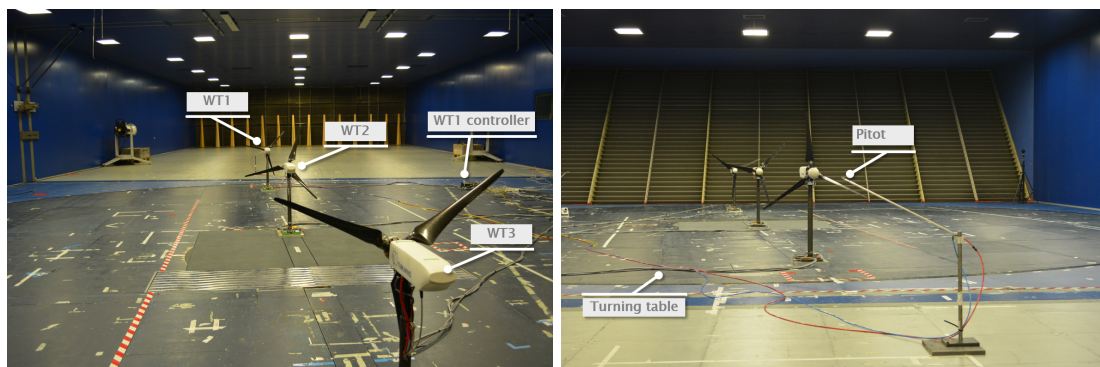


**Figure 1.** Wind farm layout in the wind tunnel.

Each G1 (see Figure 1) is equipped with a three-blades rotor whose maximum rotating speed is 850 rpm. A standard power control is implemented based on [16], with two control regions. Below rated wind speed, blade pitch angles are kept constant, while the generator torque reference follows a quadratic function of rotor speed in order to maximize energy extraction. Above rated wind speed, the generator torque is kept constant, while a proportional-integral (PI) controller is used to collectively pitch the rotor blades in order to keep the generated power at the desired level. For further details please see [6, 17, 18].

### 3. Numerical solver

#### 3.1. Flow solver

caffa3d.MBRi [19][20] is an open source finite volume code second order accurate in space and time, parallelized with MPI, in which the domain is divided in unstructured blocks of structured grids. Each grid block can be either an orthogonal Cartesian grid block or a curvilinear body fitted grid block. Nevertheless, geometrical and flow properties are always expressed in a Cartesian coordinate system, expressing flow properties in primitive variables. To provide greater geometrical flexibility, the immersed boundary method [21] can be combined with both, Cartesian and body fitted grid blocks. In addition to this, an overlapping grid technique based on [22] is implemented in the code, allowing for independent grids with higher quality where it is required.

Regarding the turbulence model, different subgrid scale models in the context of Large Eddy Simulation (LES) are implemented: the standard Smagorinsky model [23], the dynamic Smagorinsky model [24], the dynamic mixed Smagorinsky model [25] and the scale-dependent dynamic Smagorinsky model [26] with different averaging schemes.

Different wind turbine rotor models have been implemented in the code, the Actuator Disk Model with Rotation [27] and the Actuator Line Model (ALM) [28], while a torque controller and pitch controller based on [29] are used to model the wind turbines operation.

#### 3.2. Numerical setup

The size of the computational domain is 27.50 m in the streamwise direction, 5.50 m in the spanwise direction and 4.50 m in the vertical direction. It is uniformly divided in the streamwise and spanwise direction with 384 and 96 grid cells respectively, while a stretched grid is used in the vertical direction with 80 grid cells, covering one vertical rotor diameter with 30 grid cells. Two additional spatial resolutions have been tested for a stand-alone model wind turbine with the same numerical setup, obtaining an acceptable agreement with experimental data with the spatial resolution considered in this paper [30].

A zero velocity gradient is imposed at the outlet and a wall model based on the log law is used to compute the stress at the surface while periodic conditions are used in the lateral boundaries. The Crank-Nicolson scheme is used to advance in time with a time step of 0.005s and the scale dependent dynamic Smagorinsky model with a local averaging scheme is used to compute the subgrid scale stress, as in previous studies [12][13] where better results were obtained with this subgrid scale model. The inflow condition is obtained from a precursor simulation, taking into account the same numerical setup but without wind turbines and applying a periodic boundary condition in the west and east boundaries and a constant pressure gradient as forcing term.

To represent the wind turbine rotor, the ALM is used with 10 radial sections in each line. The chord and twist angle are obtained from the technical data of the model wind turbine. The airfoil used is the RG14 for the entire blade. Prandtl's tip loss correction factor is applied, as it has shown to improve the results [12]. A Gaussian smearing function (1) is used to project the aerodynamic forces onto the computational domain, taking into account three smearing parameters, one for each direction ( $n$  normal,  $r$  radial and  $t$  tangential) as described in [14].

$$f(d_n, d_r, d_t) = \frac{1}{\epsilon_n \epsilon_r \epsilon_t \pi^{1.5}} e^{-\left(\frac{d_n}{\epsilon_n}\right)^2} e^{-\left(\frac{d_r}{\epsilon_r}\right)^2} e^{-\left(\frac{d_t}{\epsilon_t}\right)^2} \quad (1)$$

The nacelle as well as the wind turbine tower are represented through drag coefficients, see for instance [27], using a 3D smearing Gaussian function to project the forces onto the computational domain.

## 4. Results

This section presents the main results obtained. First, two yaw settings are evaluated, comparing the mean streamwise velocity component at a horizontal plane 0.10 m above hub height computed in the numerical simulations with measurements of the Windscanners and the power coefficient of each model wind turbine. In the second part of this section, different yaw settings are evaluated comparing the energy capture of each wind turbine and of the whole wind farm (WF), changing the yaw offset of the first and second model wind turbines, the former from  $0^\circ$  to  $30^\circ$  and the latter from  $0^\circ$  to  $24^\circ$  with steps of  $5^\circ$  and  $4^\circ$  respectively.

### 4.1. Detail comparison of two yaw settings

Two yaw settings are analyzed, where the yaw angle of the first and second model wind turbines is  $6^\circ$  and  $5^\circ$  respectively for the first setup and  $14^\circ$  and  $11^\circ$  respectively for the second setup.

In Figure 2 the mean streamwise velocity component at different locations in the wake, measured from the upstream wind turbine and 0.10 m above hub height, is presented for yaw setting  $6^\circ/5^\circ$ . The position of each rotor centre is depicted in each subplot of the figure as a green dotted line. From the figure it can be seen that by yawing the rotor of the upstream wind turbine, the wake is deflected away from the rotor of the second wind turbine placed  $4D$  downstream. Both approaches, numerical and physical modelling, catch this. The agreement between numerical and experimental data at  $3D$  and  $4D$  is quite good, there is just an underprediction of the velocity deficit at the wake centre, may be related to the simple approach used to represent the nacelle and tower. Further downstream a similar behavior is observed, the wake is still deflected after the second model wind turbine, while downstream from the third wind turbine the shape of the wake changes because its rotor is facing the main wind direction so the larger velocity deficit is located close to its rotor centre. A very good agreement is observed between the numerical results and the experimental data.

Figure 3 depicts the mean streamwise velocity component for yaw setting  $14^\circ/11^\circ$ , in a similar fashion as Figure 2. A similar conclusion can be drawn from this figure, as the general trend of the experimental data is well captured by the numerical simulation. The wake is more deflected as expected after the first and second model wind turbines. Because of that, the shape of the wake downstream of the third wind turbine is more disturbed respect to the previous case. Despite achieving a good agreement in the wake profiles (wake width and shape) the larger velocity deficit is a bit underestimated, with larger deviations further away from the third model wind turbine.

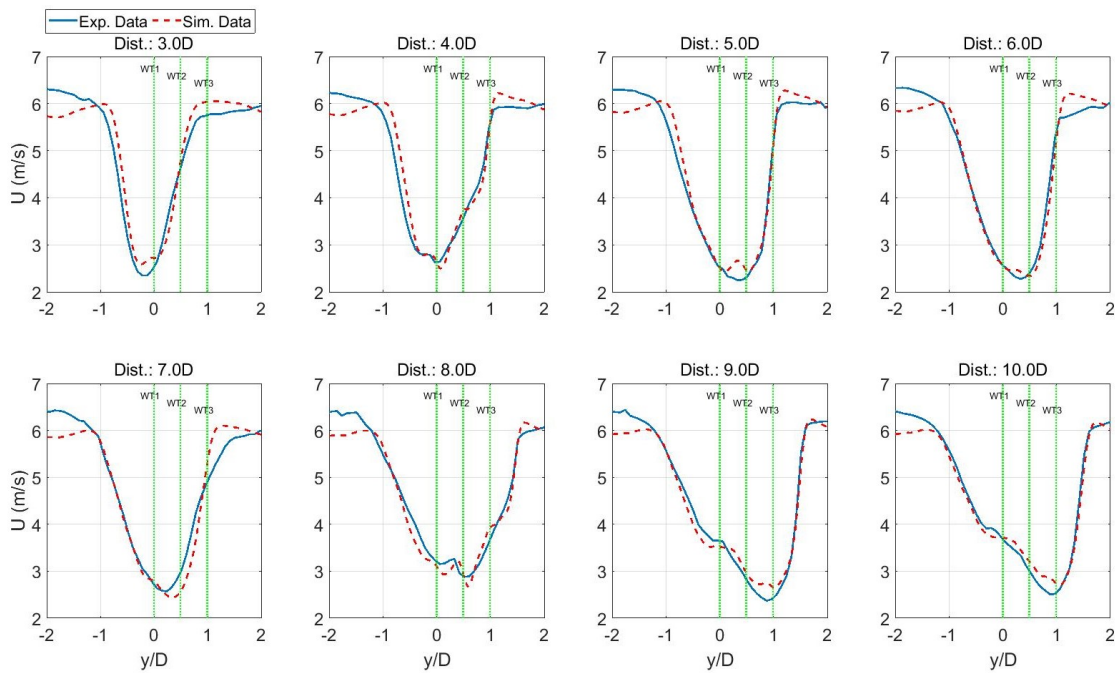


**Figure 2.** Mean streamwise velocity component at different locations in the wake, 0.10m above hub height. Exp. data: blue solid line. Sim. data: red dashed line. The dotted green lines represent the position of the wind turbine rotor centres. Yaw setup:  $6^\circ/5^\circ$ .

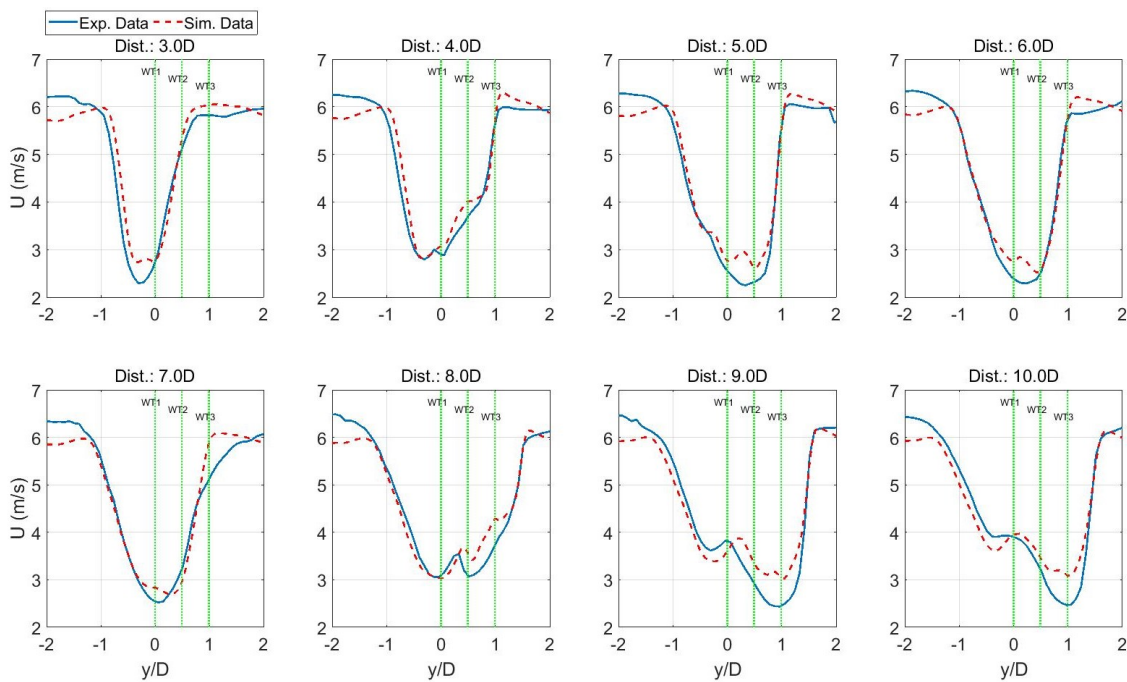


**Figure 3.** Mean streamwise velocity component at different locations in the wake, 0.10m above hub height. Exp. data: blue solid line. Sim. data: red dashed line. The dotted green lines represent the position of the wind turbine rotor centres. Yaw setup:  $14^\circ/11^\circ$ .

Regarding the energy capture, first the power coefficient of each model wind turbine and of the WF is presented for each yaw setting. The power coefficients are computed taking into account a reference wind speed of 5.67 m/s. Table 1 shows the power coefficient from the physical and numerical modelling for yaw settings  $6^\circ/5^\circ$  and  $14^\circ/11^\circ$ . The power coefficient of the upstream wind turbine is overpredicted by 5.3% for the former and by 5.8% for the latter, while for the second and third wind turbines in the row the errors are larger. A similar experimental setup is studied in [31], evaluating the influence of taking into account or not a nacelle and tower model in the simulations, finding that without a nacelle and tower model the deviations in the power coefficients are larger. In addition to this, in [32] is argued that the inflow generated by the wind tunnel is not homogeneous, with differences in the velocity up to 6%, affecting the operation of the model wind turbines. From Figure 2 and Figure 3 it can be seen that the mean streamwise velocity component outside the wake is not uniform along the spanwise direction. The deviation in the power coefficients could be related to that.

**Table 1.** Power coefficient of each model wind turbine and of the wind farm.

$C_p$	Yaw setup: $6^\circ/5^\circ$			Yaw setup: $14^\circ/11^\circ$		
	Exp. Data	Sim. Data	Difference	Exp. Data	Sim. Data	Difference
WT1	0.421	0.444	5.3%	0.409	0.433	5.8%
WT2	0.294	0.352	19.7%	0.326	0.393	20.7%
WT3	0.328	0.408	24.6%	0.377	0.436	15.8%
WF	1.043	1.204	15.4%	1.112	1.262	13.6%

From the above, the power coefficients presented below are normalized by the power coefficient of the upstream wind turbine, as a way to take into account the uncertainty related to the inhomogeneity of the wind speed along the spanwise direction. After normalizing the power coefficient, the deviations between the experimental data and the numerical results are reduced, obtaining an error of the power coefficient of the WF of 9.6% and 7.3% for yaw setups  $6^\circ/5^\circ$  and  $14^\circ/11^\circ$  respectively.

**Table 2.** Normalized power coefficient of each model wind turbine and of the wind farm.

$C_p/C_{pWT1}$	Yaw setup: $6^\circ/5^\circ$			Yaw setup: $14^\circ/11^\circ$		
	Exp. Data	Sim. Data	Difference	Exp. Data	Sim. Data	Difference
WT2	0.698	0.793	13.6%	0.796	0.909	14.1%
WT3	0.778	0.920	18.3%	0.921	1.008	9.4%
WF	2.476	2.713	9.6%	2.718	2.917	7.3%

#### 4.2. Optimal yaw setup

As mentioned in Section 1 high-fidelity numerical models have been used to evaluate the potential improvement of yawing wind turbine rotors in order to increase the overall energy capture of a wind farm, finding an optimum adjustment of the yaw offsets. Taking into account that, in this section a comparison of the optimal yaw setup of the physical modelling and of the numerical modelling is performed, as well as the improvement in energy capture respect to the greedy yaw setup in both approaches. First, the power coefficient of each model wind turbine as a function of the yaw offset of the first and second wind turbines is analyzed. As shown in Section 4.1 the power coefficients are normalized by the power coefficient of the upstream wind turbine operating without yaw offset.

#### 4.2.1. First model wind turbine in the row

Figure 4 presents the normalized power coefficient of the upstream wind turbine as a function of its yaw offset obtained in both approaches, physical and numerical modelling. The agreement between the experimental data and the numerical results is very good, observing a reduction in the energy capture when the yaw offset is increased. Generally, the dependence of the power coefficient on yaw misalignment is expressed as [33, 34]:

$$C_P(\gamma) = C_P(\gamma = 0^\circ) \cos^n(\gamma), \quad n \in [1, 3] \quad (2)$$

Figure 4 includes the adjustment obtained to the experimental and numerical data with Equation 2. The exponent  $n$  computed from the numerical data is quite close to the one computed with the experimental data.

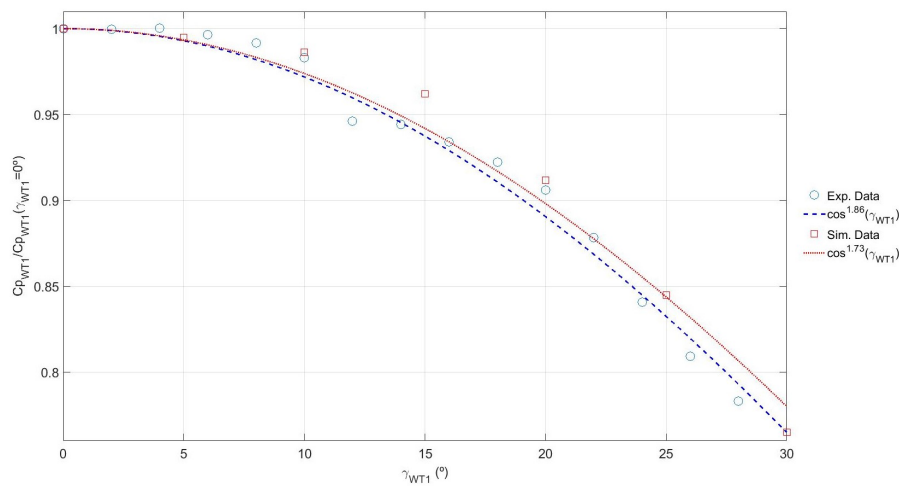


**Figure 4.** Power coefficient of the upstream model wind turbine normalized by the power coefficient without yaw offset as a function of the yaw offset. Exp. data: blue circles. Sim. data: red squares.

#### 4.2.2. Second model wind turbine in the row

In Figure 5 a similar analysis is presented, depicting the power coefficient of the second model wind turbine as a function of its yaw angle, for different values of the upstream wind turbine yaw offset, taking into account only the numerical results. From the figure, it is clear that the power coefficient of the second wind turbine depends strongly on its yaw offset as well as on the upstream wind turbine yaw offset. When adjusting the computed results taking into account Equation 2, different values of  $n$  are obtained depending on the yaw angle of the upstream wind turbine. This dependence seems to be small, nevertheless it could be taken into account when using wind farm control approaches like [3, 33]. Further investigation is needed in order to check the influence of the incoming wind on the variation of the power coefficient with the yaw angle.

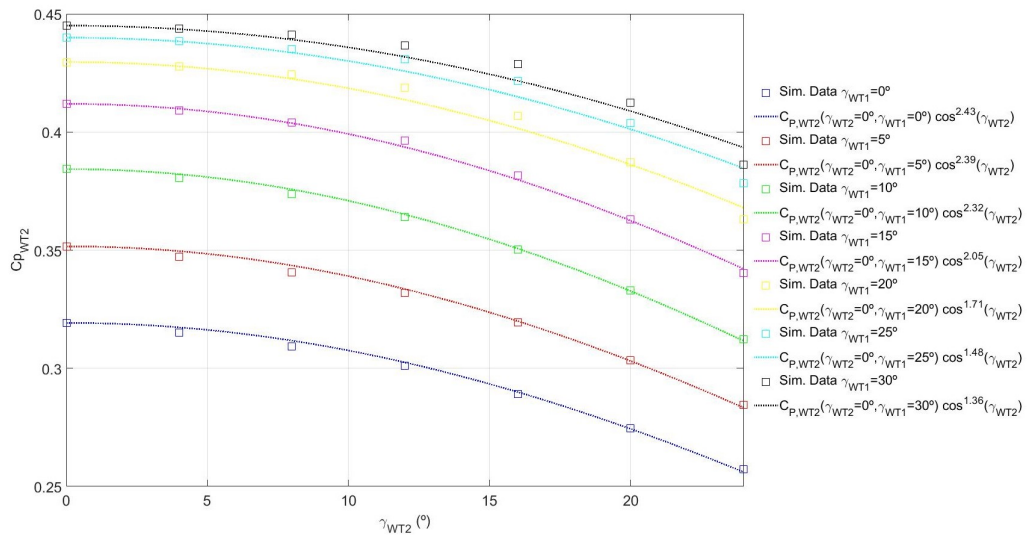


**Figure 5.** Power coefficient of the second model wind turbine in the row (WT2) as a function of its yaw offset for different yaw offset of the upstream wind turbine (WT1). Sim. data.

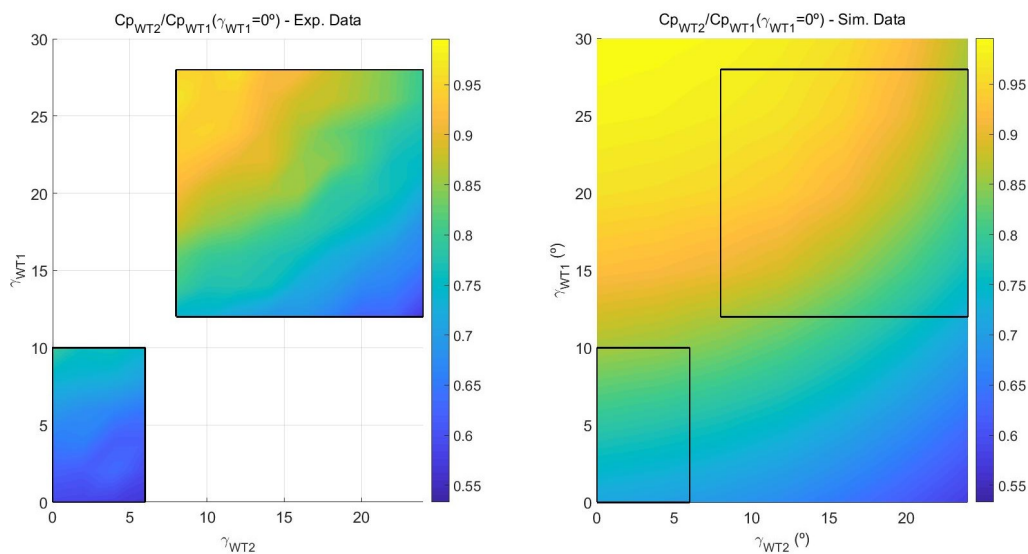


**Figure 6.** Power coefficient of the second model wind turbine in the row (WT2) normalized by the power coefficient without yaw offset of the upstream model wind turbine (WT1) as a function of the yaw offsets of the first and second wind turbines (WT1 and WT2 respectively). Exp. data: left. Sim. data: right.

As the power coefficient of the second wind turbine depends on both yaw angles, Figure 6 depicts the power coefficient normalized by the power coefficient of the upstream wind turbine without yaw offset as a function of the yaw angle of both wind turbines, comparing results from the physical and numerical modelling. In the right subplot, the range of yaw angles covered by the experimental data is represented with a solid black line. It can be seen that the general trend is well captured, the normalized power coefficient increased when decreasing the yaw offset of the second wind turbine and increasing the yaw offset of the upstream wind turbine. There

is a wider variation in the experimental data, respect to the variation in the numerical data. The reason for this is unclear and deserves further investigation, also its relationship with the inhomogeneity in the inflow wind speed of the wind tunnel mentioned in Section 4.1.

#### 4.2.3. Third model wind turbine in the row

Figure 7 presents the power coefficient of the third model wind turbine as a function of both yaw offset, normalized by the power coefficient of the first wind turbine without yaw offset. The power coefficient depends on both yaw angles, nevertheless its dependence is stronger on the yaw offset of the second wind turbine. This can be seen in both approaches: physical and numerical modelling. As mentioned before, there is a wider variation in the power coefficient obtained in the physical model respect to the variation observed in the numerical results.

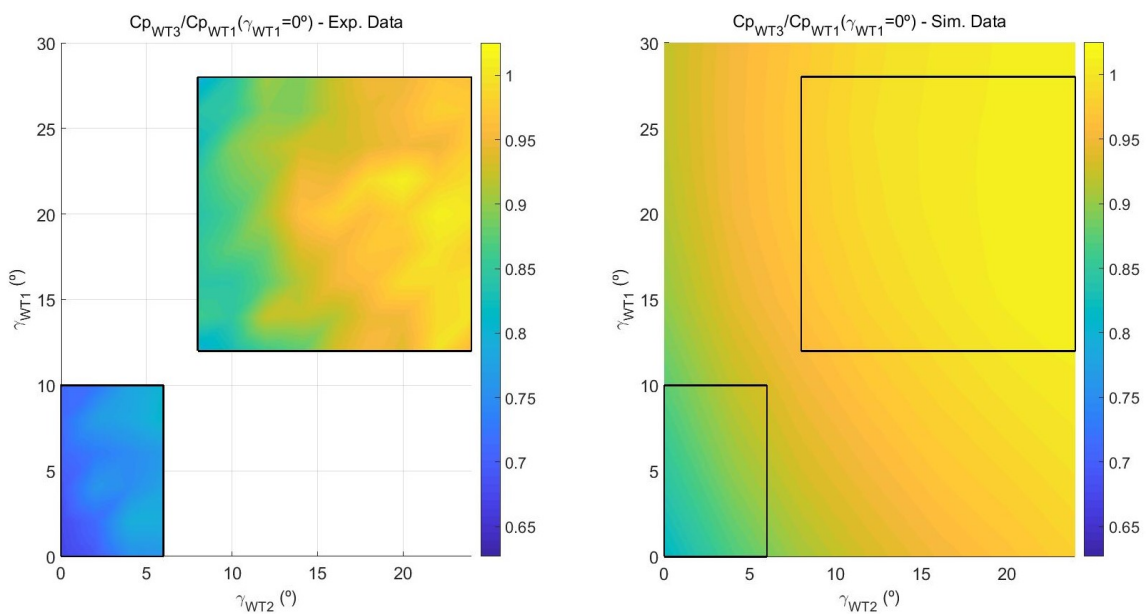


**Figure 7.** Power coefficient of the third model wind turbine in the row (WT3) normalized by the power coefficient without yaw offset of the upstream model wind turbine (WT1) as a function of the yaw offsets of the first and second wind turbines (WT1 and WT2 respectively). Exp. data: left. Sim. data: right.

#### 4.2.4. Wind farm

In this section, the power production of each model wind turbine in each yaw setting is computed and the overall power productions from the physical and numerical modelling are compared.

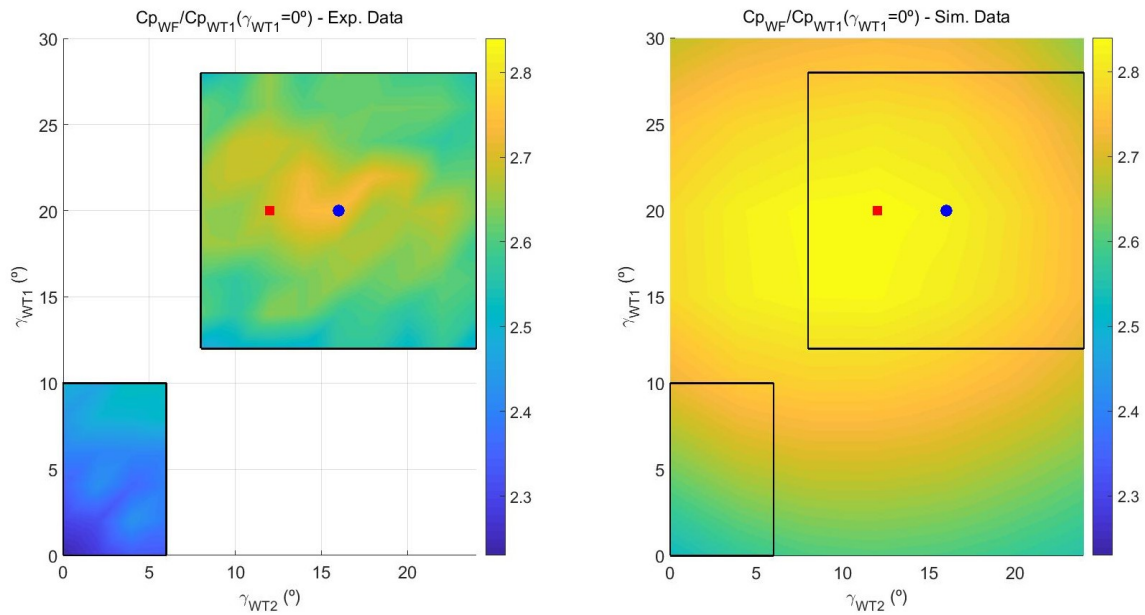


**Figure 8.** Sum of the power coefficients normalized by the power coefficient without yaw offset of the upstream model wind turbine (WT1) as a function of the yaw offsets of the first and second wind turbines (WT1 and WT2 respectively). Exp. data: left. Sim. data: right.

Figure 8 depicts the sum of the power coefficients of each model wind turbine normalized by the power coefficient of the first model wind turbine without yaw offset for both physical and numerical approaches. The blue circle represents the best experimental yaw setting tested, where the experimental wind farm power coefficient is larger, while the red square represents the best simulated yaw setting tested, where the simulated wind farm power coefficient is larger. From the figure it can be seen that the numerical framework captures with reasonable accuracy the optimum yaw configuration for this setup. The improvement in energy capture respect to the greedy setup obtained in the physical model is close to 22% while in the numerical model is close to 12%.

## 5. Conclusions

There has been an increased interest in developing control strategies at a farm level in order to maximize power production and to control active power. Regarding the former, recently it has been shown, by physical modelling or high-fidelity numerical simulations, that redirecting the wakes by yawing the wind turbine rotors is a promising strategy. This work contributes to the validation of numerical modelling of wake steering approaches against physical modelling, providing a comprehensive comparison of power output for several yaw settings obtained from both numerical and physical modelling. A configuration of three model wind turbines, separated  $4D$  in the streamwise direction and  $0.5D$  in the spanwise direction is analyzed, varying the yaw angles of the first and second wind turbines in the row. Large eddy simulation with the Actuator Line Model is used to simulate numerically the wind flow through this setup.

First, two yaw settings are assessed, evaluating the wake profile at different locations downstream from the upstream wind turbine at a horizontal plane and the power coefficients of each wind turbine. Regarding the wake profiles, a very good agreement between experimental and numerical data is obtained. However, a large deviation in the power coefficient of the second and third wind turbines is found, which could be related to the variation in the inlet condition of the wind tunnel. After normalizing the power coefficients with the power coefficient of the

upstream wind turbine, the deviations are lower, obtaining an acceptable agreement between experimental and numerical results.

Several simulations are performed in order to evaluate the influence of the yaw angle of the first and second wind turbines, particularly focused on finding the optimal yaw setup. A reasonable agreement is achieved between the power coefficients obtained in the physical model and in the numerical model, with a close agreement between the optimal yaw configurations. The general trend is well captured, despite a large deviation in the energy capture improvement of the wind farm. A wider variation is observed in the experimental data, respect to the simulated data, that deserves further investigation.

From the above results, we conclude that the numerical framework used in this paper is well suited to be used in the assessment of wind farm control strategies, particularly based on yawing the wind turbine rotors. Future research will be focused on the implementation of a hybrid approach between the one presented in [7] and in [3]. In addition to this, the influence of the flow characteristics upstream of a wind turbine in its relationship between power coefficient and yaw angle will be explored.

### Acknowledgement

This research was supported by Agencia Nacional de Investigación e Innovación (Fondo Sectorial de Energía, 2014). Computing resources were provided by Cluster-FING (Facultad de Ingeniería, Universidad de la República).

### References

- [1] International Renewable Energy Agency (IRENA) 2017
- [2] van Kuik G A M, Peinke J, Nijssen R, Lekou D, Mann J, Sørensen J N, Ferreira C, van Wingerden J W, Schlipf D, Gebraad P, Polinder H, Abrahamsen A, van Bussel G J W, Sørensen J D, Tavner P, Bottasso C L, Muskulus M, Matha D, Lindeboom H J, Degraer S, Kramer O, Lehnhoff S, Sonnenschein M, Sørensen P E, Künneke R W, Morthorst P E and Skytte K 2016 *Wind Energy Science* **1** 1–39
- [3] Gebraad P, Teeuwisse F, Wingerden J, Fleming P A, Ruben S, Marden J and Pao L 2016 *Wind Energy* **19** 95–114
- [4] Fleming P, Gebraad P M, Lee S, Wingerden J W, Johnson K, Churchfield M, Michalakes J, Spalart P and Moriarty P 2015 *Wind Energy* **18** 2135–2143
- [5] Rott A, Boersma S, van Wingerden J W and Kühn M 2017 Dynamic flow model for real-time application in wind farm control *Journal of Physics: Conference Series* vol 854 (IOP Publishing) p 012039
- [6] Campagnolo F, Petrović V, Schreiber J, Nanos E M, Croce A and Bottasso C L 2016 *Journal of Physics: Conference Series* **753** 032006
- [7] Park J, Kwon S D and Law K H 2016 A data-driven approach for cooperative wind farm control *American Control Conference (ACC), 2016* (IEEE) pp 525–530
- [8] Fleming P, Gebraad P, van Wingerden J W, Lee S, Churchfield M, Scholbrock A, Michalakes J, Johnson K and Moriarty P 2013 Sowfa super-controller: A high-fidelity tool for evaluating wind plant control approaches Tech. rep. National Renewable Energy Laboratory (NREL), Golden, CO.
- [9] Goit J P and Meyers J 2015 *Journal of Fluid Mechanics* **768** 5–50
- [10] Ciri U, Rotea M, Santoni C and Leonardi S 2016 Large eddy simulation for an array of turbines with extremum seeking control *American Control Conference (ACC), 2016* (IEEE) pp 531–536
- [11] Gebraad P M, Fleming P A and van Wingerden J W 2015 Comparison of actuation methods for wake control in wind plants *American Control Conference (ACC), 2015* (IEEE) pp 1695–1701
- [12] Draper M and Usera G 2015 *Journal of Physics: Conference Series* **625** 012021
- [13] Draper M, Guggeri A and Usera G 2016 *Journal of Physics: Conference Series* **753** 082007
- [14] Draper M, Guggeri A and Usera G 2016 *Journal of Physics: Conference Series* **753** 082028
- [15] Guggeri A, Draper M and Usera G 2017 *Journal of Physics: Conference Series* **854** 012018
- [16] Bossanyi E A 2000 *Wind energy* **3** 149–163
- [17] Bottasso C L, Campagnolo F and Petrović V 2014 *Journal of Wind Engineering and Industrial Aerodynamics* **127** 11 – 28 ISSN 0167-6105
- [18] Campagnolo F, Petrović V, Bottasso C L and Croce A 2016 Wind tunnel testing of wake control strategies *2016 American Control Conference (ACC)* pp 513–518

- [19] Usera G, Vernet A and Ferré J A 2008 *Flow, Turbulence and Combustion* **81** 471–495
- [20] Mendina M, Draper M, Soares A P K, Narancio G and Usera G 2013 *Cluster Computing* **17** 231–241
- [21] Liao C C, Chang Y W, Lin C A and McDonough J 2010 *Computers & Fluids* **39** 152–167
- [22] Hadzic H *et al.* 2006 *Development and application of finite volume method for the computation of flows around moving bodies on unstructured, overlapping grids* Ph.D. thesis Technische Universität Hamburg
- [23] Smagorinsky J 1963 *Monthly weather review* **91** 99–164
- [24] Germano M, Piomelli U, Moin P and Cabot W H 1991 *Physics of Fluids A: Fluid Dynamics* **3** 1760–1765
- [25] Zang Y, Street R L and Koseff J R 1993 *Physics of Fluids A: Fluid Dynamics* **5** 3186–3196
- [26] Porté-Agel F, Meneveau C and Parlange M B 2000 *Journal of Fluid Mechanics* **415** 261–284
- [27] Wu Y T and Porté-Agel F 2011 *Boundary-layer meteorology* **138** 345–366
- [28] Sørensen J N and Shen W Z 2002 *Journal of Fluids Engineering* **124** 393
- [29] Jonkman J, Butterfield S, Musial W and Scott G 2009 Definition of a 5-mw reference wind turbine for offshore system development Tech. rep. National Renewable Energy Laboratory (NREL), Golden, CO.
- [30] Draper M, Guggeri A, Mendina M, Usera G and Campagnolo F *Manuscript under review*
- [31] Wang J, McLean D, Campagnolo F, Yu T and Bottasso C L 2017 *Journal of Physics: Conference Series* **854** 012047
- [32] Wang J, Foley S, Nanos E M, Yu T, Campagnolo F, Bottasso C L, Zanotti A and Croce A 2017 *Journal of Physics: Conference Series* **854** 012048
- [33] Schreiber J, Nanos E, Campagnolo F and Bottasso C 2017 Verification and calibration of a reduced order wind farm model by wind tunnel experiments *Journal of Physics: Conference Series* vol 854 (IOP Publishing) p 012041
- [34] Medici D 2005 *Experimental studies of wind turbine wakes: power optimisation and meandering* Ph.D. thesis KTH